

Comparison of Bayesian Land Surface Temperature algorithm performance with Terra MODIS observations

John A. Morgan
The Aerospace Corporation
P. O. Box 92957
Los Angeles, CA 90009

Abstract

An approach to land surface temperature (LST) estimation that relies upon Bayesian inference has been validated against multiband infrared radiometric imagery from the Terra MODIS instrument. Bayesian LST estimators are shown to reproduce standard MODIS product LST values starting from a parsimoniously chosen (hence, uninformative) range of prior band emissivity knowledge. Two estimation methods have been tested. The first is the iterative contraction mapping of joint expectation values for LST and surface emissivity described in a previous paper. In the second method, the Bayesian algorithm is reformulated as a Maximum *A-Posteriori* (MAP) search for the maximum joint *a-posteriori* probability for LST, given observed sensor aperture radiances and *a-priori* probabilities for LST and emissivity.

Two MODIS data granules each for daytime and nighttime were used for the comparison. The granules were chosen to be largely cloud-free, with limited vertical relief in those portions of the granules for which the sensor zenith angle $|ZA| < 30^\circ$. Level 1B radiances were used to obtain LST estimates for comparison with the Level 2 MODIS LST product.

The agreement of LST estimates obtained by both algorithms with the MODIS LST values is good: For all four granules, the mean discrepancy $\langle \Delta T \rangle < 1\text{ K}$, and its standard deviation does not exceed 1 K . Of note, 68% confidence intervals for the LST uncertainty associated with assumed uncertainty in surface emissivity are of order 1.5 K .

The Appendix presents a proof of convergence of the iterative contraction mapping algorithm. The expectation values of surface temperature in multiple bands, and jointly in all bands, converge to a fixed point, within a stipulated convergence criterion. The fixed point exists independently of the

accuracy of the resulting LST estimate, but in certain cases is unique. In the event that the support for the calculation of the expectation value is constrained to bracket the maximum in the posterior probability for LST, the fixed point converges to the MAP LST estimate as the number of iterations grows without bound.

1. Introduction

Land surface temperature (LST) is a vitally important remotely observable tracer of mass and energy exchange across the interface between the atmosphere and the ground. LST is of interest in its own right for local climate studies and climate change monitoring, and as a component of studies of land cover, land cover change, surface moisture, and precision farming, among others (Dash et al., 2002; Wan et al., 2004). Unfortunately, few surfaces at the bottom of the atmosphere radiate as blackbodies, and the parameterization of their surface state by means of emissivities complicates the task of accurate temperature determination.

This paper continues the development of Bayesian LST estimators that do not require accurate knowledge of surface emissivity, given radiance in multiple bands (Morgan, 2005). The approach may be considered as complementary to the widespread use of regression-law based split-window algorithms. The context for the development is infrared radiometry, but the analysis can be adapted to other regions of the electromagnetic spectrum.

Section 2 reviews the elements of the Bayesian LST formalism. Two implementations of the Bayesian approach have been investigated. The first is the iterative contraction mapping algorithm presented in Morgan (2005). The second is a Maximum-A Posteriori approach to LST estimation. Section 3 presents Bayesian estimates of LST and band emissivity for MODIS imagery. Section 4 discusses results, and a final Section 5 offers conclusions. The Appendix present a proof of convergence for the iterative algorithm, and estimates of the effect on LST retrieval of uncertainty in aerosol loading.

2. Elements of Bayesian Land Surface Temperature Estimation

2.1. *The Posterior Probability for T*

We begin by recalling some of the results obtained in Morgan (2005), which may be consulted for details. The probability of sensing radiance I_i

at the top of the atmosphere (TOA), given T, ϵ_i , and an estimate σ_i of the variance of the sensor radiance noise, is obtained by a Maximum Entropy (MAXENT) argument. The MAXENT estimator assumes the existence of a forward model for the TOA radiance in terms of T and ϵ_i . For the case of a sensor aperture radiance forward model I_i^{FM} that is *linear* in band emissivity ϵ_i , the posterior probability

$$P(I_i | T, \epsilon_i, \sigma_i) \quad (1)$$

is Gaussian in the mismatch between I_i and I_i^{FM} in each band i . We also have

$$P(\{I_i\} | T, \{\sigma_i\}) = \prod_{i=1}^N P(I_i | T, \epsilon_i, \sigma_i). \quad (2)$$

as the posterior probability for all bands jointly.

Given radiance I_i in N bands detected at the top of the atmosphere (TOA) that originates from a patch on the Earth's surface by a sensor with noise radiance σ_i , the posterior probability that the surface is at a temperature T is given by Bayes' theorem as

$$P(T, \epsilon_i | I_i, K) = P(T, \epsilon_i | K) \frac{P(I_i | T, \epsilon_i, K)}{P(I_i | K)}. \quad (3)$$

Equation (3) is evaluated with aid of the prior probability for the surface to be at temperature T and emissivity ϵ_i given available knowledge K ,

$$P(T, \epsilon_i | K) dT d\epsilon_i \propto \frac{dT}{T} d\epsilon_i, \quad (4)$$

The result is a posterior probability density. If one is ignorant of, or unconcerned with, the value of emissivity, it is possible to marginalize on the nuisance variable ϵ_i :

$$P(T | I_i, K) = \int_{\epsilon_{min}}^{\epsilon_{max}} d\epsilon_i P(T, \epsilon_i | I_i, K) \quad (5)$$

and $P(T | I_i, K)^1$ may be expressed in closed form using error functions. The explicit form is given in Morgan (2005).

¹In Morgan (2005), the posterior probability density was written $P(T | I_i, K) \frac{dT}{T}$

2.2. Land Surface Temperature Algorithms

We desire to find an estimator for surface temperature using the posterior probability given by Bayes' Theorem (3). Two LST algorithms have been developed. The first, recounted in Morgan (2005), iteratively computes expectation values of LST and band emissivities from their posterior probabilities while contracting the range of *a-priori* limits on these parameters.

The second calculational method is search for the maximum *A-Posteriori* probability (MAP) value of LST that maximises $P(T | I_i, K)$. The motivation for investigating a MAP formulation for the Bayesian LST estimator is simple. The original Bayesian LST algorithm presented in Morgan (2005) obtains estimates of LST and band emissivity by iterative refinement of expectation values for these quantities. Even though the posterior probability for surface T is a closed-form expression, this procedure is computationally intensive. Moreover, extensions to the estimator such as, for example, a more careful treatment of the forward model, or incorporation of calibration error effects (Morgan, 2006), may deprive us of the comfort of the closed-form solution. The MAP criterion for an estimator promises to dramatically reduce the number of CPU cycles expended per LST estimate, and may yet preserve the ability to rely upon closed-form solutions, at least in part. MAP LST estimates are obtained simply and quickly by a Golden Section search.²

It was conjectured in Morgan (2005), but not shown, that the iterative algorithm converges in general. The Appendix presents a proof that the iterative algorithm converges, and, in the limit, converges to the MAP estimate of LST. Granted the robustness of the Golden Section search, the existence of a solution for the MAP estimator may not appear to be a concern. However, the MAP algorithm in general includes iterative refinement of the *a-priori* limits on surface emissivity. The existence of a unique MAP estimate for LST in that case follows from a straightforward adaptation of the method of proof given in the Appendix.

2.3. Confidence Intervals

A desirable feature of an LST estimator relying upon input sensor data unavoidably contaminated with noise and other forms of statistically random

²It is not difficult to extend the MAP approach to higher dimensions by simultaneously optimizing with Powell's method on (for example) band emissivity prior limits and LST. Sample tests of such extensions show promise, but remain to be investigated systematically.

errors is some means of estimating one’s confidence in the accuracy of individual estimates. In the present case, in which LST estimates are obtained by marginalizing over imperfectly known surface emissivities, it is of great interest to explore means of judging the effect of an uninformative range for the *a-priori* probability for ϵ_i . Direct numerical integration of the posterior probability $P(T \mid I, K)$ with respect to T was used to calculate emissivity prior confidence intervals for LST retrievals presented in this study. On the assumption that LST uncertainties arising from an uninformative emissivity prior are independent of those originating other sources of error, the emissivity prior confidence level may be combined with an estimate of the net effect of all other sources of error by adding in quadrature, to obtain an overall LST uncertainty estimate.

3. Application to MODIS imagery

Both the MAP and iterative versions of the Bayesian algorithm have been applied to MODIS imagery. The validation effort took advantage of the availability of Level 1b calibrated radiances and Level 2 land surface temperatures (used in lieu of ground truth) for Terra MODIS data granules through the EOS/DAAC website <http://daac.gsfc.nasa.gov/MODIS> (Savtchenko et al., 2004). Level 2 atmospheric profiles were obtained from the same site. The Level 2 surface temperature product is used in preference to the standard Level 3 product because it is in the same 1 km swath format as the Level 1 b radiance data. The GSFC-supplied HDFlook display package was used to manipulate the data granules and associated standard products.

Four MODIS data granules were selected for comparison of Bayesian LST estimates with the MOD11_L2 LST product. To the extent possible, granules were chosen to have large areas with gentle topographic relief and minimal cloud cover effects. A list of the granules used in this study appears in Table 1. Two granules are daytime, and two nighttime. The nighttime granule for 2006 day-of-year (DOY) 258 includes the alluvial plains of Iraq and both the coastal plains and central plateau of Saudi Arabia. 2006 DOY 268, also nighttime, includes the Great Plains portion of Central Canada. 2006 DOY 350 is a daytime dataset covering Northeast Africa, including large plains in Sudan. 2006 DOY 347, also daytime, covers much of the plains of Central Asia. The MOD11_L2 product reported LST values for approximately 75% or more of the pixels in all four granules.

Cloud-free pixels for which Level 2 MODIS LST values were reported were selected for analysis. A number of cuts were made in selecting data from the MODIS products for validation of surface temperature estimation. The use of Level 1b radiance products combined with Level 2 atmospheric profiles to generate LST for comparison with a Level 2 MODIS temperature product introduces sources of error originating in, among others, imperfect georeferencing. Thus one may expect errors in surface altitude to affect retrieval accuracy. These effects may be exacerbated by use of bilinear interpolation of 4 km horizontally reported profiles to the 1 km sampling of the spectral radiances. In order to minimize this source of potential error, LST retrieval was limited to sensor zenith angles $|ZA| < 30^\circ$. Cloudy pixels were masked by rejecting pixels for which the LST quality control mask bits 0,2,3,4, or 5 were nonzero. LST retrievals were attempted only for pixels for which the dew point temperature at the base of the water vapor profile exceeded the freezing point of water.

Cuts were also made on the basis of nonphysical or otherwise pathological fields in the granule data: Pixels for which the MODIS LST, the MODIS LST error, the surface temperature field in the profile granule (otherwise not used in the analysis), the surface air temperature at the lowest level of the profile, or the surface pressure were less than zero, were eliminated from processing. Finally, pixels for which surface pressure exceeded 1000 millibars, but for which the surface altitude was less than zero, were omitted from the analysis.

Neither ground truth nor surface meteorological range (*VSBY*) is available as a standard product with MODIS granules. However, LST derived from a split-window algorithm (Wan and Dozier, 1996; Wan, 1999) is furnished as a standard MODIS data product, and the presence of LWIR bands in the bandset used in retrievals suggests that LST retrievals should not be too sensitive to the exact value assumed for *VSBY* in the forward model. Accordingly, this study replicates MODIS LST values assuming a nominal, but fairly large, value of 23 km for the surface *VSBY* parameter for clear pixels. The Appendix presents a calculation which supports the contention that, for purposes of the present study, this approximation should not introduce large errors for clear air pixels.

A random selection of 500 pixels was made from each granule, subject to data cuts described above. LST retrievals from both MAP and two-pass iterative versions of the algorithm were obtained for all granules. In addition, $\pm 68\%$ confidence intervals were computed for the MAP retrievals by numerical integration of the posterior probability distribution. The bandset

used in the retrievals appears in Table 2. MODTRAN4 (Kniezys et al., 1996; Berk et al., 1989) was used for the forward model calculations, as described in Morgan (2005). The forward models incorporated MOD07_L2 air temperature and water vapor profiles and assumed a CO_2 mixing ratio of 382.5 ppm.

Initially, the prior probability in (4) was assumed to hold over the range

$$\begin{aligned} 200K &\leq T \leq 500K \\ 0.85 &\leq \epsilon_i \leq 0.999 \end{aligned}$$

for T and ϵ in each band. However, it proved advantageous to restrict the range of the emissivity prior for MODIS bands 31 and 32,

$$\begin{aligned} 0.95 &\leq \epsilon_{31} \leq 0.999 \\ 0.95 &\leq \epsilon_{32} \leq 0.999 \end{aligned}$$

so as to take advantage of the observation in (Wan and Dozier 1996, Wan 1999) that most natural land cover types have an emissivity in excess of 0.97 in these bands.

In the simulated LST retrievals presented in Morgan (2005), the equivalent noise radiance σ_i in each band was parameterized by a signal-to-noise ratio (SNR) value obtained by approximately inverting the noise-equivalent temperature change ($NE\Delta T$) for the specified nominal MODIS performance. Experimentation with actual MODIS data revealed that the SNR values so estimated greatly underestimated the random variance in radiance measured by the actual Terra spacecraft against real terrestrial surfaces, through a real, and sometimes dirty, atmosphere. In consequence, the SNR parameter was reduced from values characteristic of ideal performance, in which the only source of radiance error in sensor measurements is accounted for by $NE\Delta T$, by a full order of magnitude. In fact, the label "SNR" is probably somewhat misleading, since the random variability it describes is likely the concatenation of numerous confounding factors, not all of which need accurately described as "noise", but is retained because of its use in earlier studies.

The SNR values used in all retrievals reported in this study appear in Table 2. These values were selected on the basis of trial-and-error with pixels from DOY 347 that were drawn independently from the selection used for validation. LST estimates are fairly insensitive to the exact values chosen for band SNR's, so long as these are fairly large. If the SNR values are too large, the noise variance estimate becomes so tight that the retrieval becomes

pathologically overconstrained. In the most commonly observed pathology, one or more of the individual band posterior probability fails to overlap the others; *i. e.* the support of the joint posterior probability becomes the null set. If SNR is too small, $\leq O(10)$ for MODIS, LST retrievals become badly biased towards underestimates, and confidence intervals become worryingly large.

Tables 3 and 4 present the mean, standard deviation and χ^2 of the mismatch for each granule for iterative and MAP retrievals, respectively. In Table 3, summary statistics for LST are shown for

$$0.85 \leq \epsilon_{31,32} \leq 0.99 \quad (6)$$

as well as for

$$0.95 \leq \epsilon_{31,32} \leq 0.99. \quad (7)$$

On average, the mismatch with MODIS LST increases only slightly for the looser emissivity prior. Iterative and MAP performance with respect to the standard MODIS LST product appears quite similar. A small number of pixels required relaxation of the SNR parameter or emissivity priors in order to obtain an iterative LST estimate, in a pattern similar to that reported in Morgan (2005).

Table 5 shows the mean values obtained for ϵ_{31} and ϵ_{32} by backsubstitution of MAP *LST* into the posterior probability for ϵ . These may be compared³ with the ranges $\epsilon_{31} = 0.97 - 0.99$ and $-0.012 \leq \epsilon_{32} - \epsilon_{31} \leq 0.023$ for most ground cover types cited in the MOD11 algorithm theoretical basis document (Wan, 1999).

Figures 1-4 display a subset of LST retrievals compared with MODIS LST values. Figure 1 shows 200 MAP retrievals, with estimated MAP error bars obtained by adding in quadrature the confidence interval corresponding to the emissivity uncertainty prior with a net estimate of $NE\Delta T = 0.3 K$ for the MODIS sensor (Wan et al., 2004). The MODIS error bars are $\pm 0.6 K$. The best estimate of MODIS LST accuracy lies in the range $\pm 0.6 K$ to $\pm 1.0 K$ (Wan et al., 2004; Guenther et al., 2002). The discussion of MODIS LST accuracy in Wan et al. (2004) suggests an assumed LST error of $\pm 0.6 K$ will not understate the accuracy for purposes of comparison. The plots in

³Estimates of ϵ_{31} and ϵ_{32} are furnished as part of *MOD11-L2* datasets, but the values were of poor quality for the granules used in this study, precluding any meaningful comparison with the MAP estimates.

Figures 1 and 3 are limited to only 200 points for legibility. Figure 2 shows a histogram of the mismatch between the MAP estimates and MODIS LST, with the equivalent Gaussian histogram overplotted for comparison. Figures 3 and 4 show these quantities for iterative LST estimates obtained for the same 200 pixels.

Overall the accord with MODIS LST appears similar for the two algorithms. Confidence intervals for the single-pass MAP retrievals appear to be systematically somewhat larger than those for the two-pass iterative retrievals, while the standard deviation of the mismatch with MODIS LST estimates is somewhat smaller for MAP than for iterative. For both algorithms, χ^2/DOF is close to unity. Mismatch histograms in Figures 2 and 4 show departures from equivalent Gaussian histograms, but these do not appear to be gross.

Figures 5-12 display plots of the discrepancy between MAP and MODIS LST values, with $\pm 68\%$ confidence intervals, and of discrepancy histograms, for 500 MODIS pixels from each of the four data granules. Note that the confidence intervals in the plots are for the uncertainty in LST resulting from the assumed uncertainty prior for surface emissivity only, and do not (directly) reflect sensor noise effects or other sources of uncontrollable variance.⁴ The compression of the vertical scale gives a better display of the confidence intervals, while throwing the mismatch between MAP and MODIS LST retrievals into sharper relief than in Figures 1 and 3.

Despite imposition of the data cuts already described, a small number of retrievals for both algorithms have large discrepancies with respect to MOD11_L2 LST. Judging from the mismatch histograms, these appear to be outliers resulting from leakage of compromised pixels through the processing. In the case of the granule for DOY 2006/350, a single pixel out of 500 has a discrepancy in excess of $4K$. This discrepancy appears significantly out-of-family with respect to the largely Gaussian appearance and favorable χ^2 statistic for the retrievals as a whole. In Table 3, the summary statistics for DOY 350 are replicated with the single outlier pixel removed in the row marked with an asterisk, with minimal change to the overall results.

⁴These other sources of variance do enter the confidence interval through the MAXENT estimator for the mismatch between sensor and forward model radiance. Thus, the width of the confidence interval for emissivity uncertainty depends upon what value for the SNR parameter is used in the retrieval.

4. Discussion

The agreement between Bayesian LST estimates and Level 2 MODIS LST products obtained in this study is better than 1 K in both mean and standard deviation of the mismatch. MAP and iterative solutions reproduce the MODIS LST estimates comparably well. Only the DOY 347 retrieval shows a notably different mean mismatch compared to MODIS between iterative and MAP approaches.

In addition to the tendency for the Bayes LST retrievals to display a slight negative bias (consistent with the observation made in Morgan (2005)) the mismatch plots show evidence of a positive trend in the discrepancy with respect to MODIS LST. The trend is readily apparent to the eye for the daytime retrievals, but can also be discerned in Figure 7 for (nighttime) DOY 268.

Error sources arising from georeferencing errors in Level 1b radiance products have already been discussed. An additional possible origin for the discrepancies with MODIS LST is errors in the forward model. Among other causes, these could result from the fixed choice of $VSBY = 23\text{ km}$, or occur as a consequence of using erroneous values of air temperature or water vapor from the MOD07.L2 profiles in MODTRAN (Wan et al. 2004). Another possible source is imperfect cloud masking in the Level 2 MODIS products that could corrupt pixel radiances. This last source of error would afflict MODIS LST as well, and would have to affect MODIS and Bayesian LST differentially in order to contribute to discrepancies. Finally, the assumed band emissivity prior range need not always bracket the actual surface emissivity for a pixel. Nor is this list of possible sources for the discrepancy not attributable to emissivity uncertainty or noise an exhaustive catalog.

A noteworthy feature of the LST retrievals reported for this study is that the uncertainty in LST originating in the assumed lack of knowledge of surface emissivity is comparatively small, of order 1.5 K . As noted earlier, the emissivity uncertainty confidence interval depends upon the assumed level of random variance due to noise and other uncontrollable factors capable of influencing LST retrieval, but it seems likely that this observation will prove true more generally.

It was remarked earlier that the Bayesian approach to LST estimation was complementary to the more common split-window algorithmic family. The MODIS generalized split-window algorithm that furnished LST values against which performance of the Bayes approach has been tested relies upon

regression against a large training dataset, and requires assignment of pixels to emissivity classes. The Bayesian approach, while statistical in its treatment of emissivity uncertainty, relies upon radiative transfer theory, rather than regression of brightness temperatures against true LST, to invert radiance to surface temperature. It is thus a method of remotely determining LST that (so to speak) minimizes hostages to the fortunes of emissivity knowledge. The accurate reproduction in the mean of MOD11_L2 LST in this study suggests the possibility of using the Bayes approach for virtual "ground truth" to train local or regional split-window LST algorithms.

Although the golden section search for the MAP version runs faster than the iterative solution in prototype IDL code, the difference in execution time is not great, and is in any event dwarfed by the execution time for the forward model calculations in MODTRAN. However, the MAP version of the algorithm would seem preferable both on the basis of simplicity and because it readily admits extension to higher-dimensional searches for optimal joint estimates of LST and band emissivity.

5. Conclusion

The performance of the Bayesian land surface temperature retrieval algorithms has been tested by comparison of Bayesian LST estimates against the standard MODIS LST product. Both the original iterative contraction mapping search and a new Maximum A-Posteriori algorithm reproduce MODIS LST values with good accuracy. It has been shown (*vide.* Appendix) that the iterative refinement of expectation values underlying the TES algorithm presented in (Morgan 2005) converges, in general. In the limit of convergence to a unique LST estimate, the iterative approach is equivalent to the Maximum *A-Posteriori* estimator for LST.

The emissivity prior confidence intervals shown in Section 4 provide clear evidence that LST retrieval accuracy with the Bayesian approach is insensitive to modest uncertainties in surface emissivity.

Acknowledgement:

I wish to thank an anonymous referee for suggesting the Maximum-*A-Posteriori* approach.

.1. Convergence iterative LST retrieval

For reference, the expectation values for T given radiance in bands i , obtained from the joint posterior probability for observing radiances $I_i, i =$

1, N are

$$\langle T \rangle = \frac{\int_{T_{min}}^{T_{max}} TP(T | I_i, \sigma_i)}{\int_{T_{min}}^{T_{max}} P(T | I_i, \sigma_i)}, \quad (8)$$

assuming T is known to lie between a minimum and a maximum, while a joint estimator for T given radiances in all N bands is

$$\langle T \rangle = \frac{\int_{T_{min}}^{T_{max}} TP(T | \{I_i\}, \{\sigma_i\})}{\int_{T_{min}}^{T_{max}} P(T | \{I_i\}, \{\sigma_i\})} \quad (9)$$

An estimator for the emissivity in band i is given by

$$\langle \epsilon_i \rangle = \frac{\int_{\epsilon_{min}}^{\epsilon_{max}} \epsilon P(\langle T \rangle, \epsilon | I_i, \sigma_i) d\epsilon}{\int_{\epsilon_{min}}^{\epsilon_{max}} P(\langle T \rangle, \epsilon | I_i, \sigma_i) d\epsilon} \quad (10)$$

The algorithm used in Morgan (2005) iteratively refines the calculation of the expectation values (8)-(10) of surface temperature and emissivity in multiple bands by systematic contraction of the limits of integration. It has been found that this procedure, which is described in detail in (Morgan 2005), converges rapidly and reliably in practice. However, to date there has been no proof that the algorithm actually converges in general. This Appendix supplies such a proof.

.1.1. Assumptions

Both surface temperature and band emissivities are assumed to lie within limits imposed *a-priori*. The surface temperature is limited to the range

$$T_{min} \leq T \leq T_{max}. \quad (11)$$

and emissivity to the range

$$\epsilon_{min} \leq \epsilon_i \leq \epsilon_{max} \quad (12)$$

where the minimum and maximum values may be band-dependent.

.1.2. Proof of Convergence

We begin by establishing convergence for a class of contraction mappings. Consider a compact subset \mathbf{X} of \mathbf{R}^N with all elements positive, by virtue of (11). Given points $\mathbf{x}^1, \mathbf{x}^2 \in \mathbf{X}$ define a function

$$d(\mathbf{x}^1, \mathbf{x}^2) \equiv \sum_{i=1, N} |x_i^1 - x_i^2|. \quad (13)$$

The function d satisfies the positivity, reflexivity, identity and triangle inequality axioms for a metric. The pair (\mathbf{X}, d) is thus a metric space. It is also easily shown to be *complete*: The limit of any convergent sequence in \mathbf{X} is contained in \mathbf{X} . We conclude the pair (\mathbf{X}, d) is a complete metric space (Aliprantis and Burkinshaw, 1981, p. 35). We now prove a

Lemma: A contractive self-mapping on (\mathbf{X}, d) has a fixed point.

Define the function $\zeta : \mathbf{X} \rightarrow \mathbf{R}$ by

$$\zeta(\mathbf{x}) \equiv \theta \sum_{i=1, N} x_i \geq 0. \quad (14)$$

where $\theta > 1$. The domain of ζ is an open set in \mathbf{X} whenever its range is open in \mathbf{R} . The function ζ is therefore continuous and, in particular, lower semicontinuous.

Consider a contractive sequence x_i^n in \mathbf{X} with $n = 1, 2, \dots$ for which

$$x_i^n \geq x_i^{n+1}, \forall n \quad (15)$$

Define the mapping from one iterate of \mathbf{x} to another subsequent one in \mathbf{X} by

$$\mathbf{x}^m \equiv M(\mathbf{x}^n), m > n. \quad (16)$$

The domain of M is an open set whenever its range is open. Thus $M : \mathbf{X} \rightarrow \mathbf{X}$ is continuous. We have

$$d(\mathbf{x}^n, M(\mathbf{x}^n)) \leq \zeta(\mathbf{x}^n) - \zeta(M(\mathbf{x}^n)) \quad (17)$$

for all $\mathbf{x}^n \in \mathbf{X}$. The function ζ is lower semicontinuous and bounded from below, and M is a map from a complete metric space \mathbf{X} into itself. By Caristi's fixed-point theorem (Ok, 2007) any such mapping M has a fixed point. \square

Now apply the lemma to the joint iterative refinement of equations (8)-(10). For clarity we limit the discussion to (8) and (9). The extension to accomodate (10) is clear. A total of $N + 1$ expectation values for surface temperature is obtained at each stage of iteration. The values $\langle T_i \rangle$ comprise a vector in \mathbf{R}^{N+1} . These are confined within the subset of \mathbf{R}^{N+1} delimited by (11) that provides nonvanishing support for the integrations in the definitions (8) and (9). Call the vector of expectation values $\langle \mathbf{T} \rangle$.

Theorem: The iterative refinement of (8)-(9) converges.

At the n -th stage of iteration, $\langle \mathbf{T} \rangle$ is calculated over the range $[T_{min}^n, T_{max}^n]$

and the mismatch amongst the band LST expectation values $\langle T_i \rangle$ is scored by

$$\Delta(\langle \mathbf{T} \rangle) \equiv \max |\langle T_i \rangle - \langle T_j \rangle| \quad (18)$$

taken over all pairs of estimates. Let the set $\mathbf{X} = \{\mathbf{x}\}$ be the set of all m -tuplets of the form

$$\mathbf{x} \equiv \begin{pmatrix} T_{max}^0 - T_{min}^n \\ T_{max}^n \\ \{|\langle T_i \rangle - \langle T_j \rangle|, \forall i, j \leq N+1\} \end{pmatrix} \quad (19)$$

consistent with the overall limits (11). Here

$$m \equiv \binom{N+1}{2} + 2, \quad (20)$$

where the quantity in parentheses is the binomial coefficient. The set \mathbf{X} is compact, so all components of any sequence $\in \mathbf{X}$ are bounded. (They are all nonnegative, as well.) Take (13) for the metric. By the identical reasoning used in the Lemma, the pair (\mathbf{X}, d) is a complete metric space.

The function $\zeta : \mathbf{X} \rightarrow \mathbf{R}$ is lower semicontinuous, and $M : \mathbf{X} \rightarrow \mathbf{X}$ is continuous, on \mathbf{X} . By the Lemma, M has a fixed point, and the iterative refinement of $\langle \mathbf{T} \rangle$ converges in \mathbf{X} . Moreover, if

$$\begin{aligned} \lim_{n \rightarrow \infty} T_{min}^n &\equiv T_{min}^\infty \\ \lim_{n \rightarrow \infty} T_{max}^n &\equiv T_{max}^\infty, \end{aligned} \quad (21)$$

then

$$T_{min}^\infty \leq \langle \mathbf{T} \rangle \leq T_{max}^\infty \quad (22)$$

by the definition of $\langle \mathbf{T} \rangle$. \square

.1.3. Iterative algorithm and maximum a-Posteriori probability search

Note that, while in the limit $\Delta \rightarrow 0$ the iterative algorithm will always return an estimate $\langle \mathbf{T} \rangle$ all of whose components are equal, nothing in the result just obtained says any such estimate gives an accurate estimate of LST. However, any workable procedure for iteratively refining LST estimate *must* bracket the maximum posterior probability. In addition, the iterative mapping on \mathbf{X} has been defined to incorporate contraction of the support of

the integration (8) that defines $\langle \mathbf{T} \rangle$. In consequence, (22) limits the extent to which iterates of M can differ from each other in practice.

This last observation points to convergence of the estimates $\langle \mathbf{T} \rangle$. If the support for the computation of $\langle \mathbf{T} \rangle$ tends to zero as $\Delta \rightarrow 0$, then Cantor’s theorem (Aliprantis and Burkinshaw, 1981, p. 32) on the intersection of a nested sequence $\mathbf{y}_{n+1} \subseteq \mathbf{y}_n$ in a metric space implies that the limit of this process will be a singleton in \mathbf{X} , *i.e.*, a unique converged surface temperature estimate. By the remark made earlier, this unique limit will maximize the posterior probability. We thus have the

Corollary: In the limit $d(\mathbf{x}^n, \mathbf{x}) \rightarrow 0$, where $\forall \mathbf{x} \in \mathbf{X}$, iterative refinement of unbiased expectation values, *i.e.*, those for which $\text{supp}\langle \mathbf{T} \rangle$ brackets the maximum of the posterior probability for T , is equivalent to the Maximum *A-Posteriori* (MAP) approach, in which one searches directly for the value of T which maximizes the posterior probability (2).

This result is true of the straightforward extension of the proof given here to the case of a contractive iterative search for a fixed point for $\langle T, \epsilon_i \rangle$. Note that uniqueness of the solution is limited to the specific sequence by which the fixed point is approached. To the extent that a deterministic prescription for the approach to the limit is imposed upon the search for a solution, that solution will be unique.

.2. Insensitivity of LST estimates to meteorological range

The contribution of aerosol loading of the atmosphere to the forward model radiance calculations was parameterized by specifying the surface meteorological range, or visibility (*VSBY*). This is the variable used by MODTRAN to scale aerosol extinction. The meteorological range was assumed to be 23 km for all retrievals presented in the main body. Because LST retrievals were only attempted for cloud-free pixels in what were judged to be reasonably clear air conditions, it seems reasonable to suppose that this assumption should not introduce significant error so long as few pixels have $VSBY < 23\text{ km}$. We now examine the likely validity of this assumption.

We start by adapting the analysis of Morgan (2005, 2006) to obtain the prior probability for surface meteorological range *VSBY* in the absence of any prior knowledge other than that it lies between a minimum and a maximum value, and use it to construct posterior probabilities marginalized over a range of *VSBY*. The starting point is the apparently trivial observation that the meteorological range is a *length*: Traditionally, and loosely, *VSBY* is the distance at which an observer looking horizontally at a height of two meters just

fails to discern the contrast presented by an object against the horizon. In the remote sensing of objects by electromagnetic radiation, Poincaré invariance requires that any two observers must be able to relate their description of events by a Lorentz transformation. In particular, the relation between $VSBY = V$ as observed at time t in primed and unprimed coordinate systems moving with relative velocity $v = \beta c$ with respect to each other along a stipulated line of sight (which might as well be taken to be parallel to the ground plane) is given by

$$V = \gamma(V' - \beta t') \quad (23)$$

$$t = \gamma(t' - \beta V') \quad (24)$$

where

$$\gamma = \frac{1}{\sqrt{1 - \beta^2}}. \quad (25)$$

The two observers will assign prior probabilities for the occurrence of particular values of the meteorological range

$$f(V)dV \quad (26)$$

in the unprimed system and

$$g(V')dV' \quad (27)$$

in the primed one. In order for observers to agree as to the form of the estimator, the priors must be related by

$$g(V')dV' = J^{-1}f(V)dV \quad (28)$$

where

$$J = \frac{\partial V}{\partial V'} = \gamma \quad (29)$$

is the Jacobian for the transformation between descriptions in the parameter space. Primed and unprimed observers, if equally cogent, must also agree as to the functional form of the prior probability for V , thus

$$f(V) = g(V) \quad (30)$$

leading to a form of Schröder's equation for f :

$$f(V) = \gamma f(\gamma V). \quad (31)$$

The solution of (31) gives

$$f(V) = \frac{\text{const.}}{V} \quad (32)$$

for the prior probability. We conclude that the $VSBY$ parameter, with dimensions of a length, is a scale parameter, for which the prior probability takes the Jeffreys form (32) (Jaynes, 1968).

The prior probability (32) may be inserted into an estimator for LST which marginalizes on both surface emissivity and $VSBY$ in each band i ,

$$P(T | I_i, \sigma_i) = \int_{VSBY_{<}}^{VSBY_{>}} \int_{\epsilon_{min}}^{\epsilon_{max}} P(T | I_i, \epsilon, V, \sigma_i) d\epsilon \frac{dV}{V}, \quad (33)$$

from which a joint posterior probability may be calculated as a function of LST. This quantity may be used to compute MAP estimates of LST and confidence intervals. The estimator will now be used to examine the sensitivity of LST estimates when $VSBY$ was allowed to vary over a range of values by means of an illustrative sample calculation.

LST MAP retrievals and confidence intervals as a function of $VSBY_{<}$ for one of the pixels used in the DOY 350 granule comparison with MODIS LST appear in Figure 13.⁵ The $\pm 68\%$ confidence intervals shown account for the effects of the $VSBY$ and emissivity priors only, and include no estimate of uncertainty originating from noise effects. The upper limit on the visibility prior was fixed at $VSBY_{>} = 50 \text{ km}$. The surface T prior for these retrievals was constrained to the range $306 \text{ K} \leq T \leq 317 \text{ K}$. While the values of LST and associated confidence intervals for this example shown in Figure 13 cannot be directly compared with the MAP value 311.79 K marginalized on surface emissivity alone, the limited range of surface T variation, even within the constrained T prior limits, and the tendency for the confidence intervals to converge to a fixed range (consistent with the MODIS LST value) as $VSBY$ increases, both provide empirical support for the assumption that the LST retrievals presented in the main text should not be too sensitive to the exact value of $VSBY$ used to parameterize aerosol loading in the forward model, so long as the actual $VSBY$ is great enough.

⁵A calculation for a single pixel is given because the use of nested Romberg quadratures, in which the innermost loop invokes MODTRAN, is quite computationally intensive.

References

- Aliprantis, C. S., and O. Burkinshaw. (1981) *Principles of Real Analysis*, North Holland, New York
- Berk, A., G. P. Andersen, P. K. Acharya, J. H. Chetwynd, L. S. Bernstein, E. P. Shettle, M. W. Matthew, and S. M. Adler-Golden. (1999) *MODTRAN4 User's Manual*, Air Force Research Laboratory, Hanscom AFB, MA
- Dash, P., F.-M. Göttsche, F.-S. Olesen, and H. Fischer. (2002) Land surface temperature and emissivity estimation from passive sensor data: theory and practice-current trends, *Int. J. Remote Sensing*, 23, 2563-2594
- Guenther, B., X. Xiong, V. V. Salmonson, W. L. Barnes, and J. Young. (2002) On-orbit performance of the Earth Observing System Moderate Resolution Spectroradiometer; first year of data, *Rem. Sens. Env.* 83, 16-30
- Jaynes, E. (1968) Prior Probabilities, *IEEE Trans. on Systems Science and Cybernetics*, SSC-4, 227-241
- Kniezys F., D. C. Robertson, L W Abreu, P. Acharya, G. P. Anderson, L. S. Rothman, J. H. Chetwynd, J. E. A. Selby, E. Pl Shettle, W. O. Ballery, A. Berk, S. A. Clough, and L. S. Bernstein. (1996) *The MODTRAN 2/3 Report and LOWTRAN 7 Model*, Phillips Laboratory, Hanscom AFB, MA
- Morgan, J. A. (2005) Bayesian Estimation for Land Surface Temperature Retrieval: The Nuisance of Emissivities, *IEEE Trans. Geosci. Remote Sensing*, 43, 1279-1288
- Morgan, J. A. (2006) A Bayesian Estimator for Linear Calibration Error Effects in Thermal Remote Sensing, *IEEE Geosci. and Remote Sensing Letters*, 3 (1), 117
- Ok, E. A. (2007) *Real Analysis with Economic Applications*, Princeton University Press, Princeton, p. 238
- Savtschenko, A., D. Ouzounov, S. Ahmad, J. Acker, G. Leptoukh, J. Kosiana, and D. Nickless. (2004) Terra and Aqua MODIS products available from NASA GES DAAC, *Advances in Space Research*, 34, 710-714

- Wan, Z.-M. (1999) *MODIS Land-Surface Temperature Algorithm Theoretical Basis Document*, Institute for Computational Earth System Science, University of California, Santa Barbara
- Wan, Z., and J. Dozier. (1996) A Generalized split-window algorithm for retrieving land-surface temperature from space, *IEEE Trans. Geosci. Remote Sens.*, 34, no. 4, 892-905
- Wan, Z., Y. Zhang, Q. Zhang, and Z.-L. Li. (2004) Quality assessment and validation of the MODIS global land surface temperature, *Int. J. Remote Sensing*, 25, 261-274

Table 1. MODIS granule datasets used in validation

MOD021KM.A2006258.1900.005.2006260185940.hdf
MOD021KM.A2006268.0455.005.2006270054543.hdf
MOD021KM.A2006347.0615.005.2006348125833.hdf
MOD021KM.A2006350.0830.005.2006352011824.hdf
.....
MOD11_L2.A2006258.1900.004.2006259185248.hdf
MOD11_L2.A2006268.0455.004.2006269162220.hdf
MOD11_L2.A2006347.0615.004.2006349135340.hdf
MOD11_L2.A2006350.0830.004.2006351140447.hdf
.....
MOD07_L2.A2006258.1900.005.2006260192510.hdf
MOD07_L2.A2006268.0455.005.2006270062431.hdf
MOD07_L2.A2006347.0615.005.2006348132045.hdf
MOD07_L2.A2006350.0830.005.2006352015143.hdf

Table 2. MODIS band definitions, SNR parameters

MODIS band	wavelength limits	SNR
20	3.660-3.840 μ	25
22	3.929-3.989 μ	25
23	4.020-4.080 μ	25
29	8.400-8.700 μ	25
31	10.870-11.280 μ	50
32	11.770-12.270 μ	50

Table 3. Maximum A-Posteriori surface temperature results: mean mismatch, standard deviation, maximum mismatch, and χ^2 . Results are given for two choices for the lower limit to the emissivity prior in bands 31 and 32. The rows labeled with an asterisk differs from those immediately above it by omission of the pixel with the worst mismatch compared to MODIS LST

Granule	$\langle LST \text{ mismatch} \rangle$	$ Max \text{ mismatch} $	χ^2/DOF
<hr/>			
$0.95 \leq \epsilon_{31,32} \leq 0.99$:			
258.1900	$0.239 \pm 0.725 K$	$3.151 K$	1.106
268.0455	-0.285 ± 0.421	3.068	1.458
347.0615	-0.058 ± 0.675	2.800	1.005
350.0830	-0.040 ± 1.041	6.992	1.000
350.0830*	-0.054 ± 0.993	4.421	1.001
.....			
$0.85 \leq \epsilon_{31,32} \leq 0.99$:			
258.1900	$0.455 \pm 0.738 K$	$3.163 K$	1.378
268.0455	-0.210 ± 0.430	2.90	1.236
347.0615	0.096 ± 0.734	3.284	1.015
350.0830	0.214 ± 1.110	8.831	1.035
350.0830*	0.197 ± 1.042	4.963	1.034

Table 4. Iterative surface temperature results: mean mismatch, standard deviation, maximum mismatch, and χ^2

Granule	$\langle LST \text{ mismatch} \rangle$	$ Max \text{ mismatch} $	χ^2/DOF
<hr/>			
258.1900	$0.263 \pm 0.690 K$	$2.856 K$	1.143
268.0455	-0.295 ± 0.425	3.220	1.480
347.0615	-0.670 ± 0.966	4.081	1.480
350.0830	0.038 ± 1.355	7.789	0.999

Table 5. Mean MAP emissivities for MODIS bands 31 and 32 ($\epsilon_{max} = 0.999$)

Granule	ϵ_{min}	$\langle \epsilon_{31} \rangle$	$\langle \epsilon_{32} \rangle$
258.1900	0.85	0.961 ± 0.011	0.957 ± 0.014
268.0455	"	0.976 ± 0.002	0.975 ± 0.004
347.0615	"	0.972 ± 0.005	0.967 ± 0.008
350.0830	"	0.966 ± 0.007	0.957 ± 0.009
.....			
258.1900	0.95	0.976 ± 0.002	0.976 ± 0.002
268.0455	"	0.980 ± 0.001	0.980 ± 0.002
347.0615	"	0.979 ± 0.002	0.978 ± 0.002
350.0830	"	0.977 ± 0.002	0.975 ± 0.002

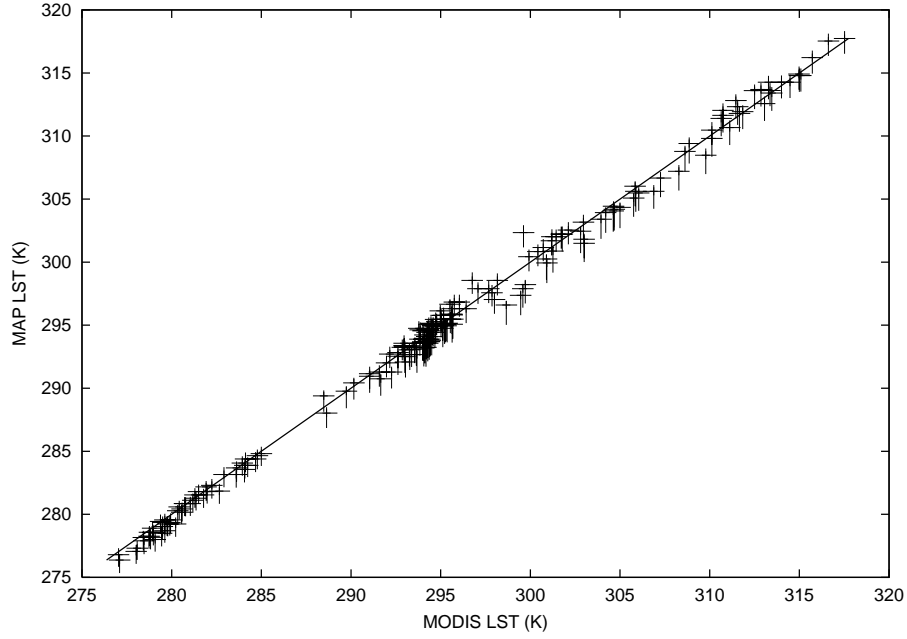


Figure 1: 200 MAP LST estimates vs. MODIS LST: 100 each daytime and nighttime.
 $\langle \delta T \rangle = -0.066K \pm 0.655K$; $\chi^2/DOF = 1.005$

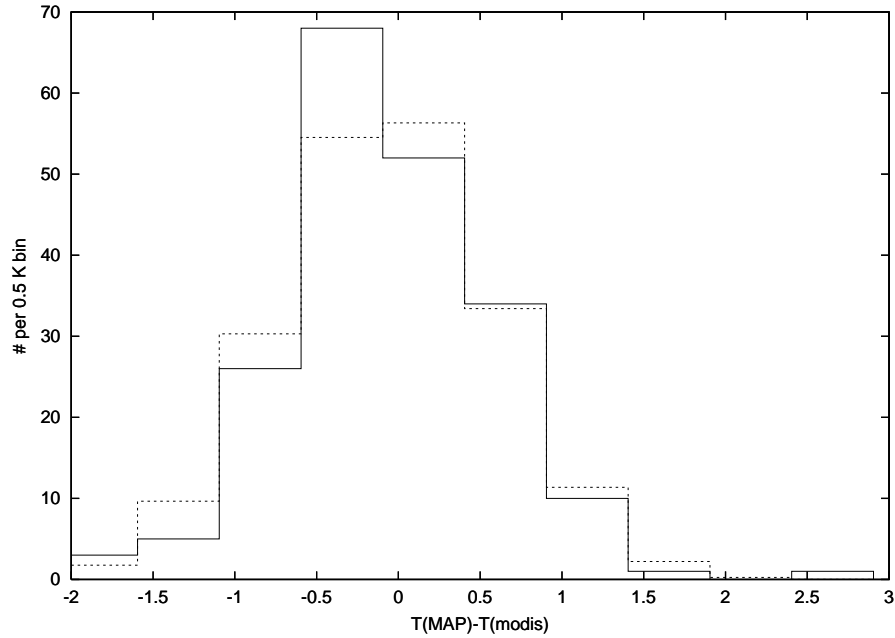


Figure 2: MAP vs. MODIS LST mismatch histogram. Solid line: MAP-MODIS mismatch; dashed line: equivalent Gaussian histogram

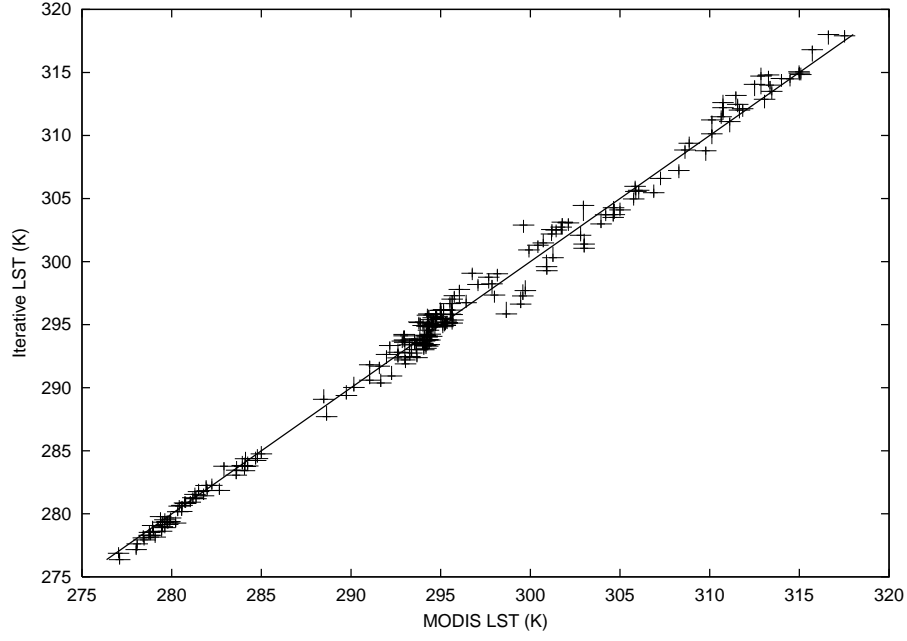


Figure 3: 200 Iterative LST estimates vs. MODIS LST.: 100 each daytime and nighttime.
 $\langle \delta T \rangle = 0.043K \pm 0.915K$; $\chi^2/DOF = 0.997$

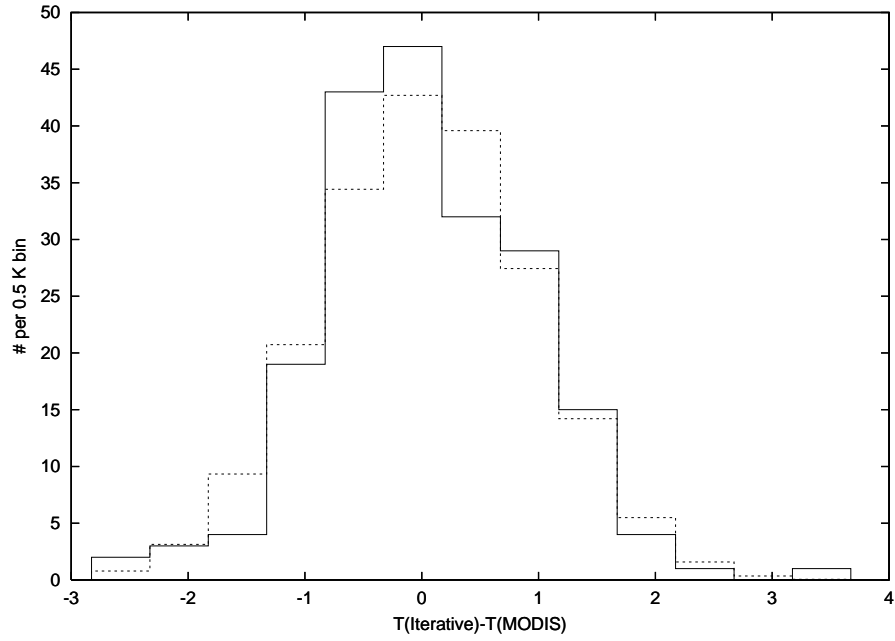


Figure 4: Iterative vs. MODIS LST mismatch histogram

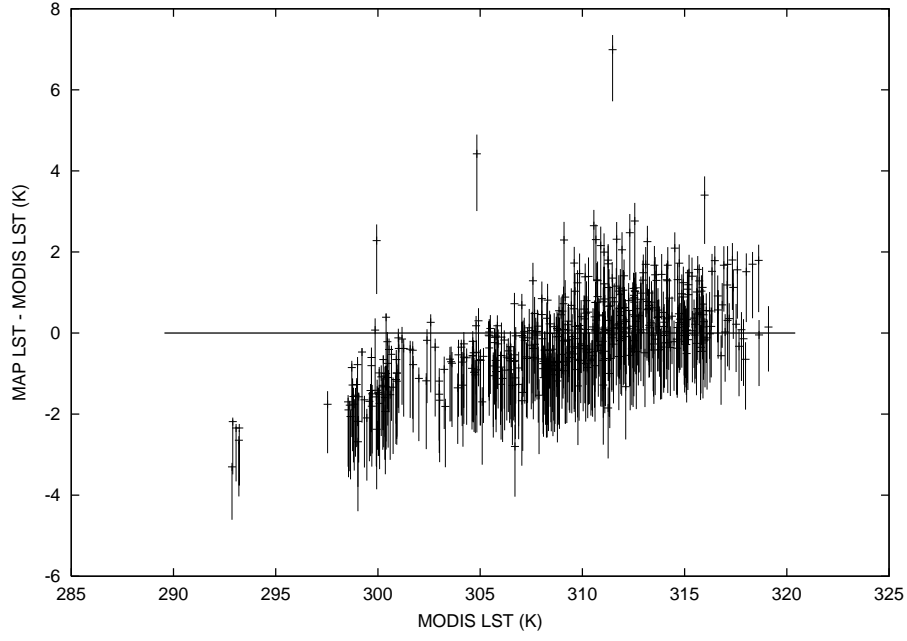


Figure 5: Mismatch between MAP and MODIS LST for 500 daytime pixels from DOY 2006/350 granule. Confidence intervals reflect effects of emissivity uncertainty only.

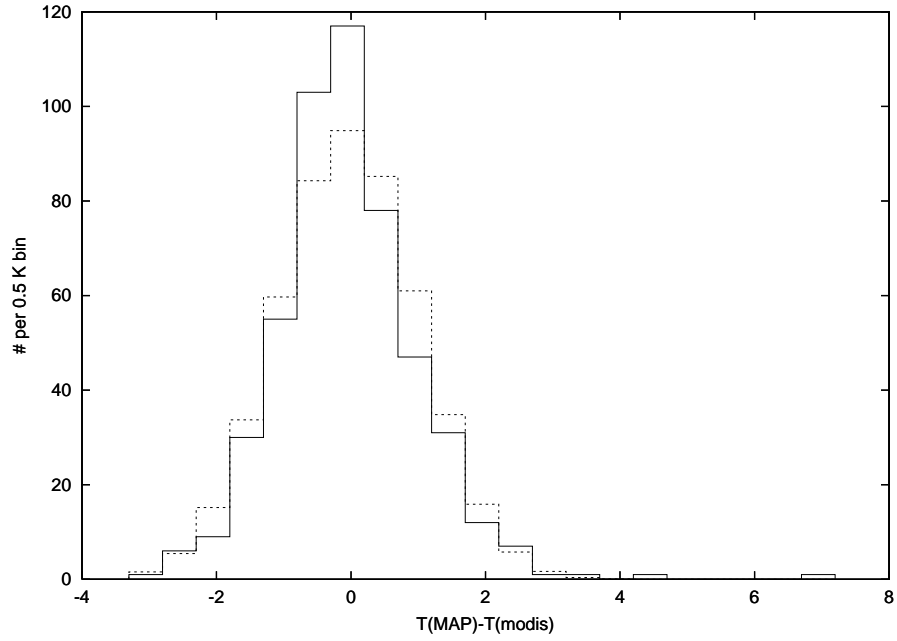


Figure 6: Daytime MAP vs. MODIS LST mismatch histogram for DOY 2006/350

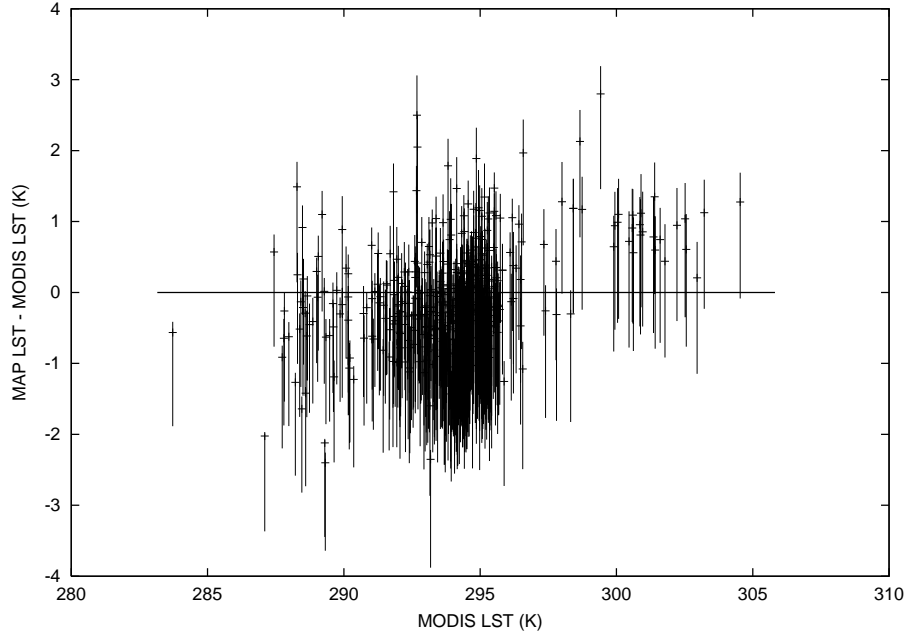


Figure 7: Mismatch between MAP and MODIS LST for 500 daytime pixels from DOY 2006/347 granule

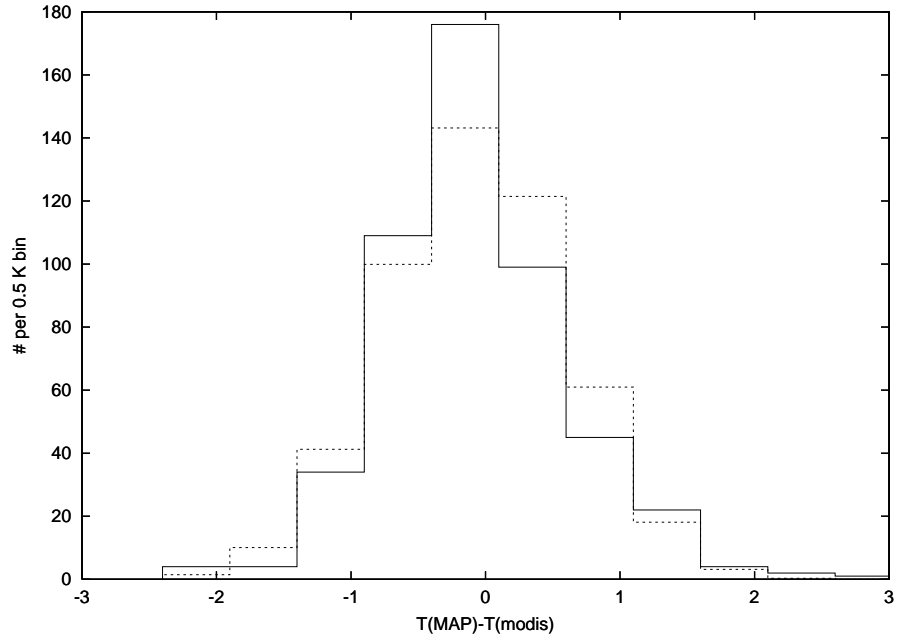


Figure 8: Daytime MAP vs. MODIS LST mismatch histogram for DOY 2006/347

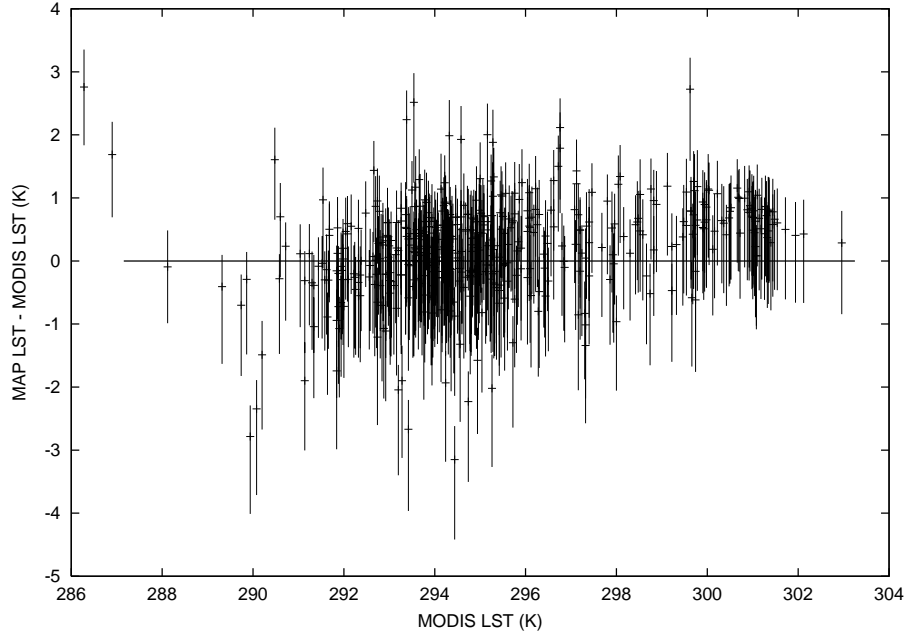


Figure 9: Mismatch between MAP and MODIS LST for 500 nighttime pixels from DOY 2006/258 granule

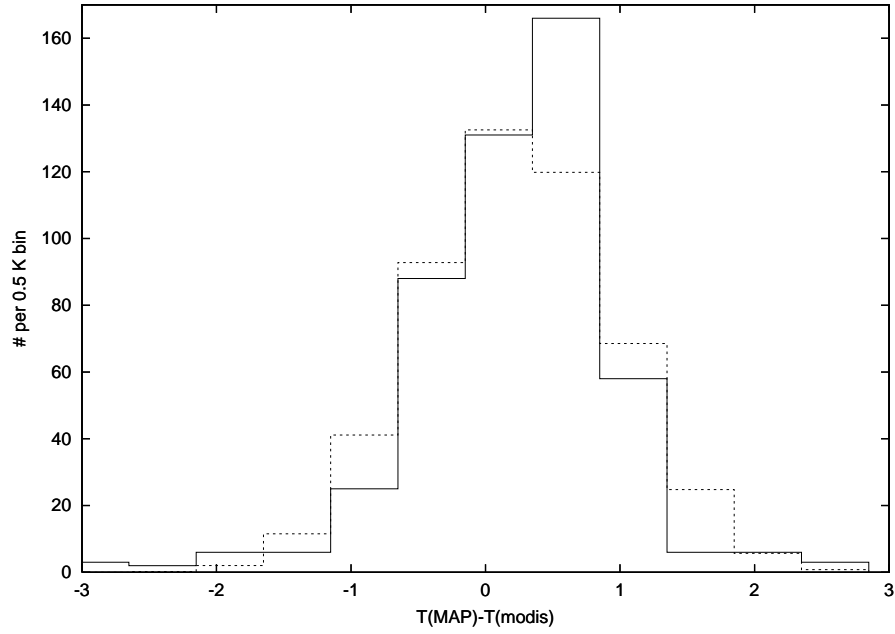


Figure 10: Nighttime MAP vs. MODIS LST mismatch histogram for DOY 2006/258

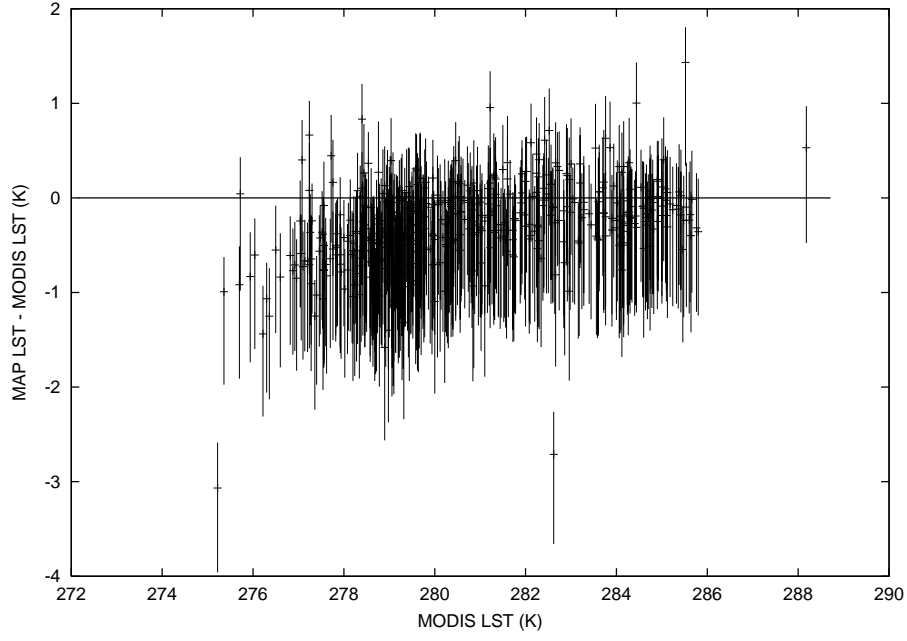


Figure 11: Mismatch between MAP and MODIS LST for 500 nighttime pixels from DOY 2006/268 granule

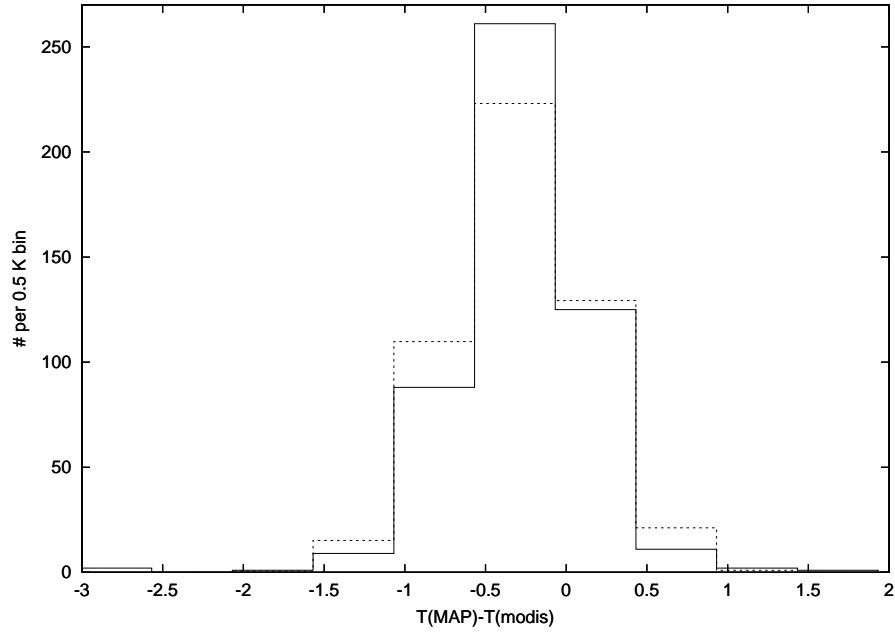


Figure 12: Nighttime MAP vs. MODIS LST mismatch histogram for DOY 2006/268

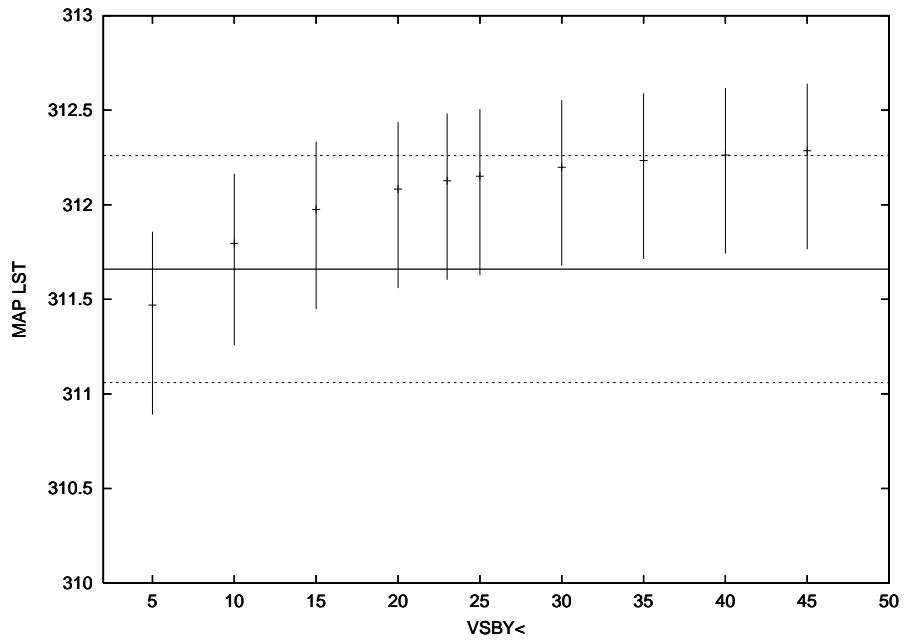


Figure 13: MAP LST estimates, confidence intervals marginalized on emissivity and $VSBY$ vs. $VSBY_{<}$ for DOY 2006/350. The horizontal lines show the MODIS LST value $311.66 \pm 0.6K$ for this pixel.